

The Microwave Background Bispectrum Paper II: A Probe of the Low Redshift Universe

David M. Goldberg and David N. Spergel
Princeton University Observatory, Princeton, NJ 08544

September 14, 2018

Abstract

Gravitational fluctuations along the line-of-sight from the surface of last scatter to the observer distort the microwave background in several related ways: The fluctuations deflect the photon path (gravitational lensing), the decay of the gravitational potential produces additional fluctuations (ISW effect) and scattering off of hot gas in clusters produce additional fluctuations (Sunyaev-Zel'dovich effect). Even if the initial fluctuations generated at the surface of last scatter were Gaussian, the combination of these effects produce non-Gaussian features in the microwave sky. We discuss the microwave bispectrum as a tool for measuring a studying this signal. For MAP, we estimate that these measurements will enable us to determine the fraction of ionized gas and to probe the time evolution of the gravitational potential.

1 Introduction

Over the past few years, cosmologists have emphasized that measurements of the two-point correlation function of CMB anisotropies can yield a wealth of information about physical conditions in the early universe. In this article, we will discuss how non-linear physics can produce a detectable non-Gaussian

signature in the microwave background. We concentrate on cases in which gravitational lensing between here and the surface of last scatter couple via a Limber's equation to produce a non-Gaussian signal. The amplitude of this signal is sensitive to the evolution of gravitational potential fluctuations at low redshift. Thus, measurements of the non-Gaussianity will complement measurements of the two point correlation function by providing information about physical conditions in the low-redshift universe.

In §2, we discuss cross-correlating the effects of gravitational lensing and the Integrated Sachs-Wolfe (ISW) effect and cross-correlating the effects of gravitational lensing with the Sunyaev-Zel'dovich (SZ) effects. Because there are equal numbers of hot and cold spots, gravitational lensing alone does not produce a detectable three-point signal[1]. However, the combination of lensing with other low redshift effects will produce an observable non-Gaussian signature. In §3, we compute the signal/noise for this effect and discuss these cosmological applications. A companion paper[2] provides a more general discussion of the bispectrum, including derivation of the angle-averaged bispectrum, a method for measuring the bispectrum and estimating the signal to noise, and a fully worked example of the bispectrum produced by the Rees-Sciama effect.

2 Computing the Bispectrum

The angle-averaged bispectrum is the spherical harmonic transform of the temperature three point function,

$$\begin{aligned}
 B_{l_1 l_2 l_3} &= \sum_{m_1 m_2 m_3} \begin{pmatrix} l_1 & l_2 & l_3 \\ m_1 & m_2 & m_3 \end{pmatrix} \int d\hat{\mathbf{l}} d\hat{\mathbf{m}} d\hat{\mathbf{n}} \langle T(\hat{\mathbf{l}}) T(\hat{\mathbf{m}}) T(\hat{\mathbf{n}}) \rangle \\
 &\times Y_{l_1 m_1}^*(\hat{\mathbf{l}}) Y_{l_2 m_2}^*(\hat{\mathbf{m}}) Y_{l_3 m_3}^*(\hat{\mathbf{n}}) ,
 \end{aligned} \tag{1}$$

where $T(\hat{\mathbf{n}})$ is defined as the temperature anisotropy (with mean zero) at a particular point in the sky. We expand the temperature out into three terms:

$$T(\hat{\mathbf{n}}) = \sum_{lm} a_{lm} Y_{lm}(\hat{\mathbf{n}}) + \sum_{lm} a_{lm} \nabla \Theta(\hat{\mathbf{n}}) \cdot \nabla Y_{lm}(\hat{\mathbf{n}}) + T_{lr}(\hat{\mathbf{n}}) \tag{2}$$

where the first term is the CMB fluctuations from the surface of last scatter, the second term describes the effects of lensing and the third term describes

the effects of secondary processes at low redshift. We shall assume throughout this paper that the third term is first order (e.g. $\propto \Phi_0(\mathbf{k})$), but clearly, second order secondary processes would also give rise to an observable bispectrum, as is the case with the Rees-Sciama effect considered in the companion paper[2]. For this article, we will consider two sources of secondary anisotropy (both of which are first order), the ISW effect and the Sunyaev- Zel'dovich effect.

Combining equations (1) and (2) yields,

$$\begin{aligned}
B_{l_1 l_2 l_3} &= \sum_{m_1 m_2 m_3} \begin{pmatrix} l_1 & l_2 & l_3 \\ m_1 & m_2 & m_3 \end{pmatrix} \int d\hat{\mathbf{l}} d\hat{\mathbf{m}} d\hat{\mathbf{n}} Y_{l_1 m_1}^*(\hat{\mathbf{l}}) Y_{l_2 m_2}^*(\hat{\mathbf{m}}) Y_{l_3 m_3}^*(\hat{\mathbf{n}}) \\
&\times \sum_{l' m m'} Y_{lm}(\hat{\mathbf{l}}) \langle a_{lm} a_{l'm'}^* \rangle \langle \nabla \Theta(\hat{\mathbf{m}}) \cdot \nabla Y_{l'm'}^*(\hat{\mathbf{m}}) T_{lr}(\hat{\mathbf{n}}) \rangle
\end{aligned} \quad (3)$$

plus an additional 5 terms representing the various permutations of the observation angles.

We can immediately integrate over $\hat{\mathbf{l}}$:

$$\begin{aligned}
B_{l_1 l_2 l_3} &= \sum_{m_1 m_2 m_3} \begin{pmatrix} l_1 & l_2 & l_3 \\ m_1 & m_2 & m_3 \end{pmatrix} \int d\hat{\mathbf{m}} d\hat{\mathbf{n}} Y_{l_2 m_2}^*(\hat{\mathbf{m}}) Y_{l_3 m_3}^*(\hat{\mathbf{n}}) \\
&\times c_{l_1} \langle \nabla \Theta(\hat{\mathbf{m}}) \cdot \nabla Y_{l_1 m_1}^*(\hat{\mathbf{m}}) T_{lr}(\hat{\mathbf{n}}) \rangle
\end{aligned} \quad (4)$$

We may note that by integrating by parts:

$$\begin{aligned}
\int d\hat{\mathbf{m}} \nabla^2 Y_{l_3 m_3}^*(\hat{\mathbf{m}}) \Theta(\hat{\mathbf{m}}) Y_{l_1 m_1}^*(\hat{\mathbf{m}}) &= - \int d\hat{\mathbf{m}} \nabla Y_{l_2 m_2}^*(\hat{\mathbf{m}}) \cdot \nabla \Theta(\hat{\mathbf{m}}) Y_{l_1 m_1}^*(\hat{\mathbf{m}}) \\
&- \int d\hat{\mathbf{m}} \nabla Y_{l_2 m_2}^*(\hat{\mathbf{m}}) \cdot \nabla Y_{l_1 m_1}^*(\hat{\mathbf{m}}) \Theta(\hat{\mathbf{m}})
\end{aligned} \quad (5)$$

where the surface integrals drop out, since we are integrating over a complete unit sphere. Combining this expression, with similar expressions involving the Laplacian of $\Theta(\hat{\mathbf{m}})$ and $Y_{l_1 m_1}^*(\hat{\mathbf{m}})$, we find:

$$\begin{aligned}
B_{l_1 l_2 l_3} &= \frac{1}{2} \sum_{m_1 m_2 m_3} \begin{pmatrix} l_1 & l_2 & l_3 \\ m_1 & m_2 & m_3 \end{pmatrix} \int d\hat{\mathbf{n}} Y_{l_3 m_3}^*(\hat{\mathbf{n}}) c_{l_1} \\
&\times \int d\hat{\mathbf{m}} \left\langle \left[\nabla^2 Y_{l_2 m_2}^*(\hat{\mathbf{m}}) \Theta(\hat{\mathbf{m}}) Y_{l_1 m_1}^*(\hat{\mathbf{m}}) \right. \right. \\
&- \left. \left. Y_{l_2 m_2}^*(\hat{\mathbf{m}}) \nabla^2 \Theta(\hat{\mathbf{m}}) Y_{l_1 m_1}^*(\hat{\mathbf{m}}) - Y_{l_2 m_2}^*(\hat{\mathbf{m}}) \Theta(\hat{\mathbf{m}}) \nabla^2 Y_{l_1 m_1}^*(\hat{\mathbf{m}}) \right] T_{lr}(\hat{\mathbf{n}}) \right\rangle
\end{aligned} \quad (6)$$

Since $\Theta(\hat{\mathbf{m}})$ and $T_{lr}(\hat{\mathbf{n}})$ are scalar quantities, their expectation value will depend only on their spatial separation:

$$\begin{aligned}\langle \Theta(\hat{\mathbf{m}})T_{lr}(\hat{\mathbf{n}}) \rangle &= \sum_l \left(\frac{2l+1}{4\pi} \right) b_l P_l(\hat{\mathbf{m}} \cdot \hat{\mathbf{n}}) \\ &= \sum_{lm} b_l Y_{lm}^*(\hat{\mathbf{m}}) Y_{lm}(\hat{\mathbf{n}})\end{aligned}\quad (7)$$

Inserting equation (8) into equation (7) and integrating yields,

$$\begin{aligned}B_{l_1 l_2 l_3} &= \frac{l_2(l_2+1) - l_1(l_1+1) - l_3(l_3+1)}{2} \sqrt{\frac{(2l_1+1)(2l_2+1)(2l_3+1)}{4\pi}} \\ &\quad \times \begin{pmatrix} l_1 & l_2 & l_3 \\ 0 & 0 & 0 \end{pmatrix} c_{l_1} b_{l_3}\end{aligned}\quad (8)$$

Plus 5 additional terms, reflecting the various permutations of l_1 , l_2 and l_3 .

2.1 Cross-correlating Lensing with the ISW Effect

If the universe is not flat with $\Omega_m = 1$, then at late times, gravitational potential fluctuations decay. This decay generates additional microwave background fluctuations:

$$\begin{aligned}T^{ISW}(\hat{\mathbf{n}}) &= 2 \int_0^{\tau_0} d\tau \dot{\phi}(\tau, \hat{\mathbf{n}}\tau) \\ &= 2 \int_0^{\tau_0} d\tau \frac{d^3\mathbf{k}}{(2\pi)^3} \Phi_0(\mathbf{k}) \exp(i\mathbf{k} \cdot \hat{\mathbf{n}}\tau) \dot{\phi}(\tau)\end{aligned}\quad (9)$$

where the gravitational potential fluctuations have been expanded out in Fourier space, $\hat{\mathbf{n}}$ is the direction of photon propagation, and τ is conformal (comoving) lookback time. If a line-of-sight passes primarily through high density regions, then it will be on average hotter than lines-of-sight that pass primarily through low density regions.

Foreground fluctuations in the gravitational potential also distort the photon geodesics,

$$\begin{aligned}\vec{\theta}(\hat{\mathbf{m}}) &= 2 \int_0^{\tau_0} d\tau \frac{\tau_0 - \tau}{\tau_0} \nabla_{\perp} \phi(\tau, \hat{\mathbf{m}}\tau) \\ &= 2i \int d\tau \frac{d^3\mathbf{k}}{(2\pi)^3} k \Phi_0(\mathbf{k}) (\hat{\mathbf{k}} - (\hat{\mathbf{k}} \cdot \hat{\mathbf{m}})\hat{\mathbf{m}}) \exp(i\mathbf{k} \cdot \hat{\mathbf{m}}\tau) \phi(\tau) \frac{\tau_0 - \tau}{\tau_0} \\ &\equiv \nabla_{\perp} \Theta(\hat{\mathbf{m}})\end{aligned}\quad (10)$$

This effect is surprisingly large; a typical photon's trajectory has been deflected roughly several arcminutes from its initial path.

By measuring the three-point function, we can cross-correlate these two effects,

$$\begin{aligned} \langle T^{ISW}(\hat{\mathbf{n}})\Theta(\hat{\mathbf{m}}) \rangle &= \frac{8}{\pi} \int k^2 dk P(\mathbf{k}) \int_0^{\tau_0} d\tau \int_0^{\tau_0} d\tau' \phi(\tau) \frac{\tau_0 - \tau}{\tau\tau_0} \\ &\quad \times \dot{\phi}(\tau') \sum_{l,m} j_l(k\tau) j_l(k\tau') Y_{lm}^*(\hat{\mathbf{m}}) Y_{lm}(\hat{\mathbf{n}}), \end{aligned} \quad (11)$$

where we have used the Rayleigh expansion of the Fourier mode into spherical harmonics:

$$e^{i\mathbf{k}\cdot\mathbf{r}} = 4\pi \sum_{lm} i^l j_l(kr) Y_{lm}^*(\hat{\mathbf{r}}) Y_{lm}(\hat{\mathbf{k}}). \quad (12)$$

Since most of the contribution to the integral comes from when $\tau \simeq \tau'$, we approximate $\dot{\phi}$ by its value at that time and then integrate over τ' :

$$b_l^{ISW} = -\frac{4}{\pi^{1/2}} \frac{\Gamma\left(\frac{l}{2} + \frac{1}{2}\right)}{\Gamma\left(\frac{l}{2} + 1\right)} \int P(k) k dk \int d\tau \phi(\tau) j_l(k\tau) \dot{\phi}(\tau) \frac{\tau_0 - \tau}{\tau\tau_0} \quad (13)$$

In our analysis, we compute this integral numerically up to $l = 50$. However, for large l , we can evaluate this integral quickly by noting that $j_l(k\tau) \simeq \delta(k\tau - l) \sqrt{\pi/2l}$, yielding:

$$b_l^{ISW} \simeq -8 \int d\tau \phi(\tau) \dot{\phi}(\tau) \frac{\tau_0 - \tau}{\tau^2 \tau_0} P(l/\tau) \quad (14)$$

To illustrate the behavior of this coefficient, Figure 1 shows a plot of b_l versus l for an $\Omega_m = 0.3$, $\Lambda = 0.7$ cosmology.

2.2 Cross-correlating Lensing with the Sunyaev-Zel'dovich Effect

Filaments, groups, and clusters will distort the microwave background through both the SZ effect and gravitational lensing[3]. The amplitude of the effect depends upon the integrated pressure fluctuations along the line-of-sight,

$$T^{SZ}(\hat{\mathbf{n}}) = -\frac{2\sigma_T}{m_e c^2} \int a d\tau \delta p_e(\tau) \quad (15)$$

where σ_T is the Thompson cross-section, m_e is the electron mass and δp_e is the fluctuations in electron pressure.

The electron pressure is the product of the electron density and the electron temperature. On large scales, we parameterize this as $\delta p_e = b_{gas} \bar{p} \Delta$, where b_{gas} is the gas bias factor (which is expected to be ~ 4 as dense regions are hotter than low density regions [4]), \bar{p} is the mean gas pressure and Δ is the fluctuation in the dark matter density. This approximation only holds on scales in which linear theory holds. However, as we will show, the SZ-lensing bispectrum probes scales of $k^{-1} > 100$ Mpc. Numerical simulations (R. Cen, private communication) find that the density weighted temperature, $kT_e \simeq 1/(1+z)$ keV for $z < 3$. Since the gas density falls as $(1+z)^{-3}$, the pressure drops roughly as $(1+z)^{-2}$. Based on this, we approximate the large scale SZ fluctuations as,

$$T^{SZ}(\hat{\mathbf{n}}) = -2y_0 b_{gas} \int \frac{d\tau}{\tau_0} \frac{\Delta(\hat{\mathbf{n}}, \tau)}{a} \quad (16)$$

where $y_0 = \sigma_T n_{e0} k T_{e0} \tau_0 / m_e c^2$. For a flat universe with $H_0 = 65 \text{ km/s}$, and $\Omega_{ionized} = 0.05$ $T_{e0} = 1$ keV, $y_0 = 1.2 \times 10^{-5}$. This approximation is likely to be valid on scales larger than the non-linear scale.

We can relate the dark matter density to the potential and rewrite equation (16),

$$T^{SZ}(\hat{\mathbf{n}}) = \frac{4y_0 b_{gas}}{3H_0^2 \Omega_m} \int \frac{d^3 \mathbf{k}}{(2\pi)^3} k^2 \Phi_0(\mathbf{k}) \int \frac{d\tau}{\tau_0} \phi(\tau) e^{i\mathbf{k} \cdot \hat{\mathbf{n}} \tau} \quad (17)$$

and now compute the *SZ - lensing* cross-correlation term:

$$\begin{aligned} \langle T^{SZ}(\hat{\mathbf{n}}) \Theta^*(\hat{\mathbf{m}}) \rangle &= \frac{16y_0 b_{gas}}{3\pi H_0^2 \Omega_m} \int dk k^4 P(k) \int d\tau d\tau' \phi(\tau) \phi(\tau') \frac{\tau_0 - \tau}{\tau \tau_0^2} \quad (18) \\ &\times \sum_{lm} j_l(k\tau) j_l(k\tau') Y_{lm}^*(\hat{\mathbf{m}}) Y_{lm}(\hat{\mathbf{n}}) \end{aligned}$$

As l gets large, the spherical Bessel functions can be treated as approximating delta functions such that:

$$j_l(k\tau') \simeq \delta(l - k\tau') \frac{\sqrt{\pi} \Gamma(\frac{l}{2} + \frac{1}{2})}{2 \Gamma(\frac{l}{2} + 1)} \quad (19)$$

Making this approximation for τ' and integrating from $-\infty$ to ∞ yields:

$$b_l^{SZ} \simeq \frac{8y_0 b_{gas}}{3\pi^{1/2} H_0^2 \Omega_m} \frac{\Gamma(\frac{l}{2} + 12)}{\Gamma(\frac{l}{2} + 1)} \int dk k^3 P(k) \phi(l/k) \int d\tau \phi(\tau) \frac{\tau_0 - \tau}{\tau \tau_0^2} \quad (20)$$

This may be further simplified by making the same approximation for $j_l(k\tau)$ and integrating over k :

$$b_l^{SZ} \simeq \frac{8y_0 b_{gas} l^2}{3H_0^2 \Omega_m} \int d\tau \phi^2(\tau) \frac{\tau_0 - \tau}{\tau^5 \tau_0^2} P(l/\tau) \quad (21)$$

Note that for very small values of τ (low redshift), $P(l/\tau) \propto \tau^{-7}$, and the kernel of the above equation goes to 0. It is only in the large wavelength regime in which $P(k) \propto k^{-5}$ where the integral is maximized. This occurs around $\Lambda = 100h^{-1}\text{Mpc}$ for most cosmological models, and thus, the assumption that pressure and density perturbations are proportional and evolve linearly are well motivated.

As Figure 1 shows, the Sunyaev-Zel'dovich effect dominates over the ISW effect at large l . Since the SZ effect is enhanced by non-linear evolution, the estimated signal in equation (21) is likely an underestimate, numerical simulations, complemented by improved analytical techniques, will be needed to more accurately compute the signal.

It may be thought that b_l will merely change normalization with a change of Ω_m , and thus, $y_0 b_{gas}$ (which clearly only affects the normalization) and Ω_m would be indistinguishable. Since there is little variation in c_l for variations of Ω_m , it might be thought that the bispectrum *shape* will be roughly constant, and thus, only the normalization could be extracted. In Figure 2, we show that this is not the case. For variations in Ω_m , we see that b_l varies not only in normalization, but in shape as well, and thus, both $y_0 b_{gas}$ and Ω_m will be able to be extracted almost independently.

3 Discussion

Will we be able to detect either effect? We can estimate this by determining whether in a $\Omega_m = 0.3, \Omega_\Lambda = 0.7$ universe, we can use the MAP data to reject the hypothesis that there is no non-Gaussianity in the CMB maps:

$$\chi^2 = \sum_{l_1, l_2, l_3} \frac{\langle B_{l_1, l_2, l_3} \rangle^2}{\langle B_{l_1, l_2, l_3}^2 \rangle} \quad (22)$$

where we restrict the sum to $l_1 < l_2 < l_3$. For our standard set of parameters, $\chi^2 \simeq 9$ with most of the signal coming from the SZ effect. Thus, measuring the bispectrum will enable us to measure $\Omega_{ionized}$ and probe the time evolution of the gravitational potential.

In Figure 3, we plot the value of χ^2 for the ISW-lensing bispectrum for flat models with varying Ω_m and Ω_Λ . As shown in the Figure, the PLANCK[5] satellite will do an excellent job differentiating between the null hypothesis and a given value of Ω_m , giving a 4σ signal for $\Omega_m = 1.0$. The MAP satellite, however, will be unable to differentiate between the two.

Likewise, this method will be able to potentially probe different equations of state. While the Cosmological constant behaves as a component with $w \equiv P/\rho = -1$ (our fiducial model), different equations of state produce dramatically different rates of potential growth, and hence, we may measure the χ^2 difference between test values of w and $w = -1$, as shown in Figure 4. Note that both MAP and PLANCK provide constraints on w at the 1σ level; PLANCK gives $w < -0.8$, and MAP gives $w < -0.4$.

As seen in Figure 3, MAP will be sensitive to this effect as well, and the 4 year results will yield 1σ uncertainties of $\delta\Omega_m = \pm 0.4$. PLANCK can distinguish SZ from CMB fluctuations, so it will be very sensitive to this effect as well. However, calculating its signal to noise is beyond the scope of this paper.

Figure 5 shows the additional χ^2 for a mode with a given value of l_3 (by convention, the largest index). Note that the maximal contribution occurs near $l_3 = 900$ for PLANCK. Though the SZ-lensing effect is generally at higher mode numbers (see the comparison between the signals as will be detectable by MAP), it will nevertheless produce a much stronger signal in MAP than will the ISW-lensing effect, since at high l (but less than 600), the SZ-lensing coefficient (b_l) dwarfs the coefficient for the ISW-lensing effect (see Figure 1).

In this article, we estimated the non-Gaussian signature produced by the combined effects of gravitational lensing and the ISW effect and the combined effects of gravitational lensing and the SZ effect. For most cosmological models, the SZ signature is stronger and will swamp the ISW effect signal. Detecting the SZ-lensing cross-correlation will determine the mean density of ionized gas in the today's universe. Thus, MAP should be able to detect the "missing baryons" [6, 7].

By cross-correlating the MAP data with observations of large scale struc-

ture and X-ray maps, we can look for additional signatures of low redshift physics. Previous papers have discussed cross-correlating the galaxy distribution in the Sloan Survey with the temperature maps to look for gravitational lensing effects[8] and for the Sunyaev-Zel'dovich produced by both clusters and superclusters[9]. Boughn et al.[10] have looked for cross-correlations between the cosmic X-ray and microwave backgrounds in an attempt to detect the late-time ISW effect. Combining these different cross-correlations will enable cosmologists to determine the relationship between the mass distribution and the distribution of gas and galaxies. These observations will also probe the time evolution of the gravitational potential and provide a new tool for measuring the basic cosmological parameters.

4 Acknowledgments

We thank Alex Refregier, Jeremy Goodman, Martin Bucher, Gary Hinshaw, Arthur Kosowsky and Dick McCray for useful discussions. We also thank Uros Seljak and Matias Zaldarriaga for sharing their results prior to publication. DNS acknowledges the MAP/MIDEX project for support. DMG is supported by an NSF graduate research fellowship.

5 References

References

- [1] F. Bernardeau., *Astron. Astrophys.* **338**, 767 (1998).
- [2] D. N. Spergel & D. M. Goldberg, Paper I, submitted to *Phys. Rev. D* (1999).
- [3] J. P. Ostriker, & E. T. Vishniac, *Nature* **322**, 804 (1986).
- [4] A. Refregier, D.N. Spergel, & U. Pen, in preparation (1999).
- [5] <http://astro.estec.esa.nl/PLANCK/>
- [6] M. Fukugita, C.J. Hogan, & P.J.E. Peebles, *Astrophys. J.*, **503**, 518 (1998).

- [7] R. Cen, & J.P. Ostriker, to appear in *Astrophys J* (1999).
- [8] M. Sugimotohara, T. Sugimotohara, & D.N. Spergel, *Astrophys. J.*, **495**, 511 (1998).
- [9] A. Refregier, D.N. Spergel & T. Herbig, submitted to *Astrophys. J.* (1998).
- [10] S.P. Boughn, R.G. Crittenden, & N.G. Turok, *New Astronomy*, **3**, 275 (1998).

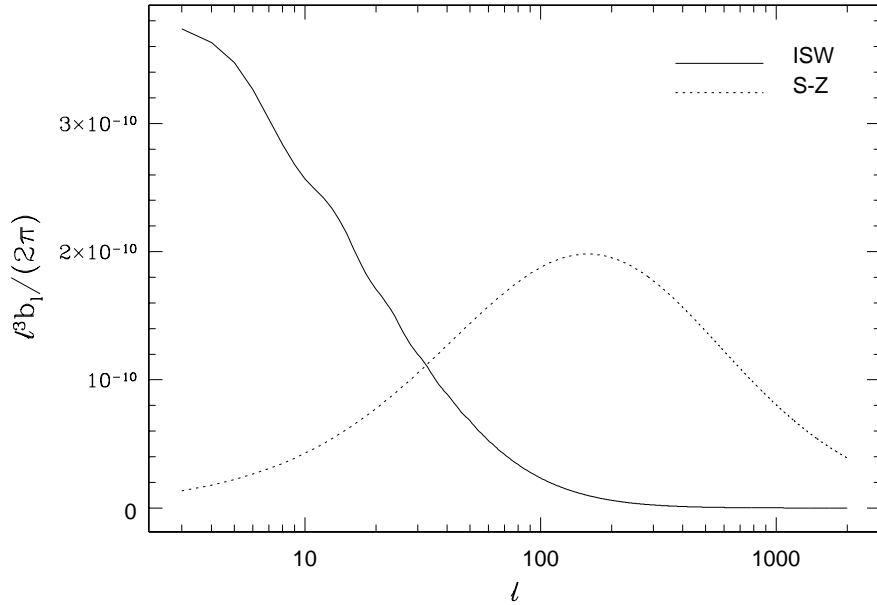


Figure 1: The b_l coefficients as a function of l . The solid line shows the coefficient from the ISW effect, while the the dashed line shows the coefficient arising from the Sunyaev Zel'dovich effect. Each of the plots is for an $\Omega_m = 0.3$, $\Omega_\Lambda = 0.7$, $h = 0.65$ cosmology. We can estimate the contribution that the different coefficients will have through dimensional analysis. Since $c_l \propto l^{-2}$, the Wigner 3-j symbols $\propto l^{-1/2}$ (equation 8) and the signal per l_3 is expected to go as $B_{l_1 l_2 l_3} \times l^{-4}$ (see equation 22) the $\chi^2/\Delta l_3$ will be roughly constant if $b_l \propto l^{-3}$. Thus we have normalized the kernels with an l^3 prefactor in order to estimate their importance.

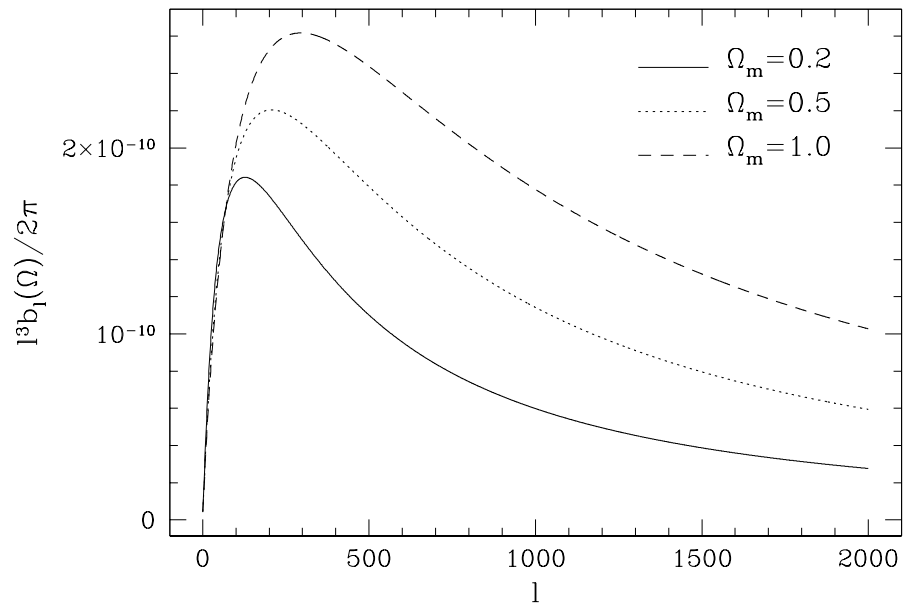


Figure 2: As in the previous figure, but the coefficients, b_l , are shown only for the SZ-lensing coupling. Here we have varied Ω_m to illustrate that the shape of the coefficients, as well as the normalization, vary with Ω_m , and thus, Ω_m cannot be considered a degenerate parameter with the product, $y_0 b_{gas}$.

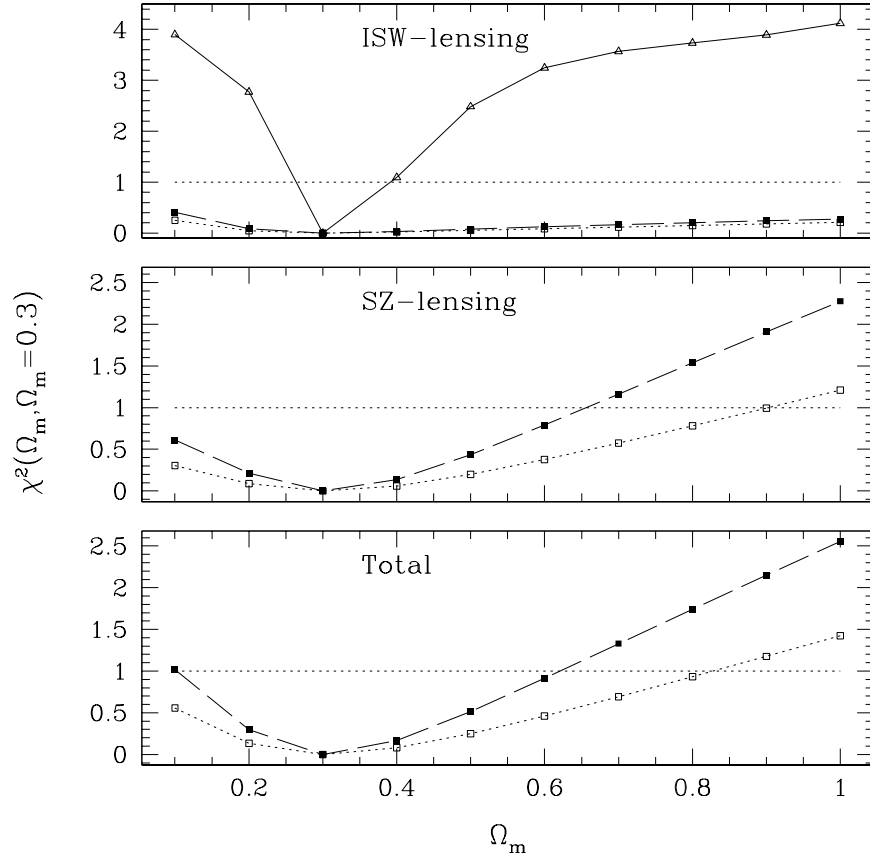


Figure 3: The χ^2 differences in the ISW-lensing bispectrum, the SZ-lensing bispectrum, and their sums between a fiducial model $\Omega_m = 0.3, \Omega_\Lambda = 0.7$ and a test model with a flat cosmology and varying Ω_m . The solid line shows the χ^2 for the PLANCK experiment, while the dashed line shows χ^2 for MAP 4 year results and the dotted line shows the MAP 1 year result. with 1 σ uncertainty.

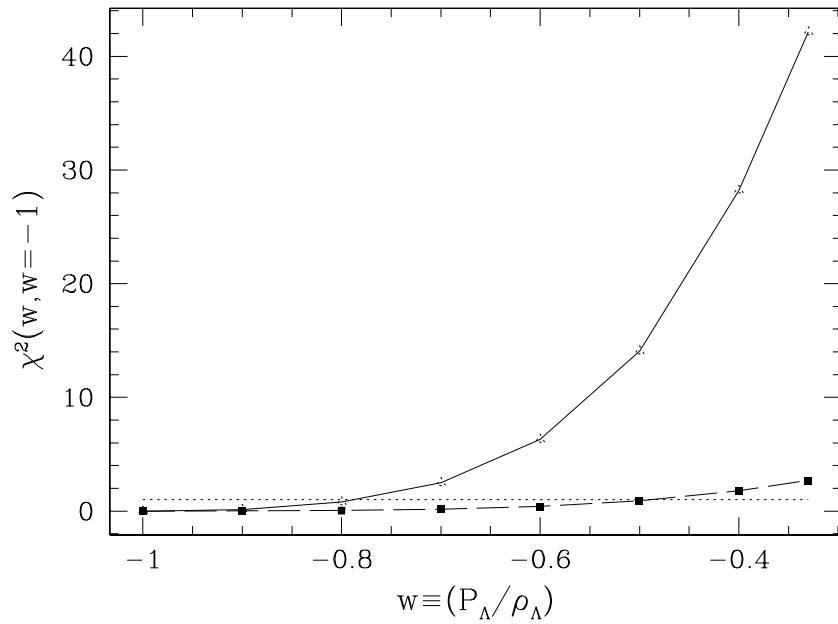


Figure 4: The same as the previous figure, but with variations in the equation, w . For a cosmological constant, $w = -1$ (our fiducial model), while $w = -1/3$ is a curvature-like term. Both MAP and PLANCK will be able to distinguish between extreme cases; MAP would predict $w < -0.4$ and PLANCK would give $w < -0.8$.

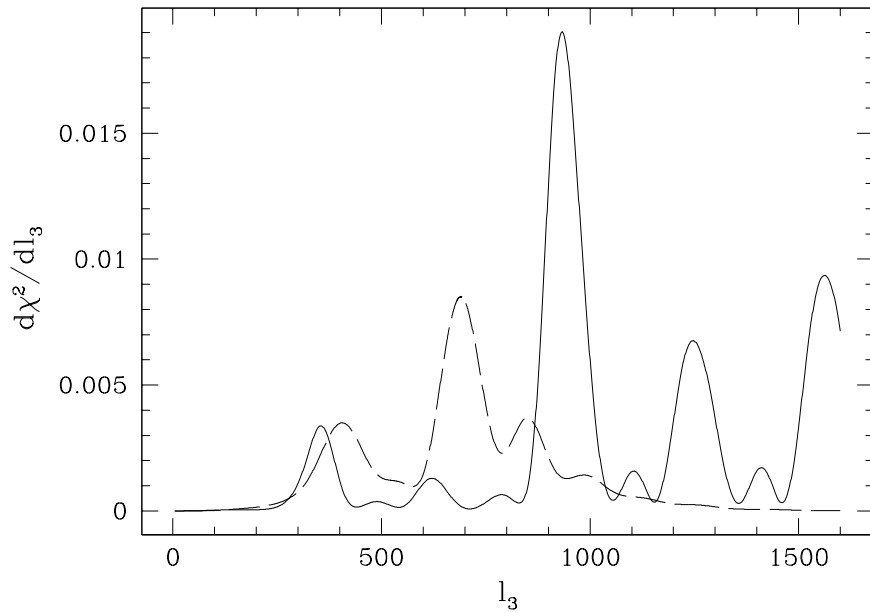


Figure 5: The χ^2 per mode (l_3) as given by the bispectrum. The solid line shows the results from the ISW-lensing effect measured by PLANCK, while the dashed line shows the SZ-lensing effect as measured by MAP (4 yr. results). In general, the signal is at higher wavenumber (smaller scale) for the SZ-lensing effect than for the ISW-lensing effect. However, PLANCK's increased sensitivity at higher wavenumber distorts this relation in this plot.